Angular position detection of single nanoparticles on rolled-up optical microcavities with lifted degeneracy

Shilong Li,[1,*] Libo Ma,[1] Stefan Böttner,[1] Yongfeng Mei,[1,2] Matthew R. Jorgensen,[1] Suwit Kiravittaya,[1,3] and Oliver G. Schmidt[1,4]

[1]*Institute for Integrative Nanosciences, IFW Dresden, Helmholtzstrasse 20, 01069 Dresden, Germany*
[2]*Department of Materials Science, Fudan University, Handan Road 220, 200433 Shanghai, China*
[3]*Department of Electrical and Computer Engineering, Faculty of Engineering, Naresuan University, Phitsanulok 65000, Thailand*
[4]*Material Systems for Nanoelectronics, Chemnitz University of Technology, Reichenhainerstrasse 70, 09107 Chemnitz, Germany*

(Received 11 October 2012; revised manuscript received 12 June 2013; published 20 September 2013)

Nanoparticle position detection is prevented in highly symmetric whispering-gallery-mode optical microcavities due to the redistributable electric field of resonant light therein. In asymmetric tubular microcavities formed by a rolled-up slab waveguide, the optical resonant modes are split and locked to the spiral-shaped geometry which provides a reference point for the nodes and antinodes of the electric field within the microcavity. The discriminative responses of neighboring resonant modes to a local disturbance provide a method for angular position detection of a single nanoparticle on a rolled-up optical microcavity. These findings add functionality to microcavity applications and a deeper understanding of cavity electrodynamics.

DOI: 10.1103/PhysRevA.88.033833 PACS number(s): 42.60.Da, 42.79.−e

I. INTRODUCTION

Optical microcavities have gained considerable attention due to the ultrahigh sensitivity of their resonant peak positions to changes in the refractive index of their surroundings [1–4]. This sensitivity is a result of strong light confinement in a small volume, leading to an extended evanescent field which overlaps with the surrounding medium. This field has been exploited for nondestructive real-time sensing applications as well as strong light-matter interactions [5–8]. Several types of optical microcavities have been investigated, including whispering-gallery structures such as microspheres [2,3], toroids [1,4–8], and other ringlike structures [9,10]. While these devices have already proven to be useful detectors, they are limited by nonselectivity if the surface is not functionalized or low versatility if it is. This problem could be overcome, greatly increasing microcavity functionality, by resolving the angular position of the analyte. An array of functionalized regions on microcavities could be used to achieve sensing of different analytes on a single microcavity.

In this article, we will discuss the importance of microcavity asymmetry on its sensing capabilities and develop a model which shows how angular position detection is possible in microcavities with well-defined asymmetric features.

Resonant modes in symmetric ring cavities, as shown in Fig. 1(a), have degenerate clockwise (CW) and counterclockwise (CCW) components [11]. In the presence of small asymmetries or nanoparticles, a reciprocal backscattering mechanism [12] leads to degeneracy lifting as shown in Fig. 1(b) [see details in Appendix]. The amplitude of the splitting is directly related to the particle size [6,7]. However, the angular position of the nanoparticles on symmetric microcavities cannot be determined from this splitting because the circumferential symmetry does not allow the definition of any reference point. Modes arising from asymmetric microcavities have been shown to be intrinsically split [13]. In this case, the positions of the split modes are locked to features of the microcavity geometry. These locked microcavity modes can be differentially perturbed by the angular position of a nanoparticle as shown in Fig. 1(c). For precise angular position detection using inherent mode splitting, a well-defined asymmetry needs to be created in the microcavity. Rolled-up microcavities can provide this requirement as their fabrication automatically leads to well-understood asymmetry resulting in split modes [14,15].

In the following, we will demonstrate how angular position detection of a single nanoparticle can be realized using the split modes in rolled-up optical microcavities. In Sec. II, we give a brief introduction of rolled-up microcavities including the fabrication method as well as basic optical properties. In Sec. III we present a variational approach to calculate the mode splitting in rolled-up microcavities which will provide the basis for our sensing model. In Sec. IV the variational model is extended to calculate the effect of a small particle on split modes based on perturbation theory. To verify our theoretical models we performed finite-difference time-domain (FDTD) simulations. The results from FDTD simulations and our theoretical models agree well with each other. In Sec. V, an approach to detect a single nanoparticle's angular position by monitoring split modes is proposed. The effect of the nanoparticle size, the axial confinement of the rolled-up microcavities, and the minimum Q factor in the coupled systems are discussed in Sec. VI. Finally, we summarize our conclusions in Sec. VII.

II. ROLLED-UP OPTICAL MICROCAVITIES

By rolling up prestrained nanomembranes [16,17], ringlike optical microcavities can be fabricated in a manner that facilitates device integration [18–23]. Optical microcavities produced in this way have excellent sensitivity as detectors due to broad evanescent fields from the subwavelength-thin walls [24]. Recently, these microcavities have been used as detectors in a variety of capacities [24,25].

*s.li@ifw-dresden.de

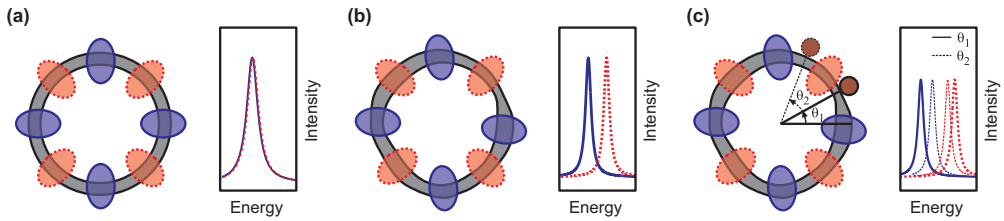

FIG. 1. (Color online) (a) Illustration of a symmetric microcavity, with accompanying degenerate CW and CCW peak components. The blue (solid line) and red (dotted line) patterns indicate their electric fields, respectively. (b) Illustration of an asymmetric microcavity; the CW and CCW components of the optical mode are locked and no longer degenerate, leading to a mode splitting, which can be perturbed by the presence of a nanoparticle as shown in (c).

One of the distinct characters of rolled-up optical microcavities is that their geometric structures are asymmetric. This asymmetry is a result of the method of their fabrication as shown in Fig. 2(a). The resulting hollow tubular structure has an asymmetric cross section, which has surfaces described as Archimedean spirals. The size of the tubular structure is controlled via the residual strain gradient and thickness of the nanomembrane [26,27]. Light confinement in this structure has been demonstrated by exciting optical modes using photoluminescence [18] or by transmission measurements based on optical fibers [28] or waveguides [29].

The flexible production of this type of microcavity allows the introduction of axial light confinement by adding a lobe structure to vary the profile in the axial direction [15]; see, for example, the details in Figs. 2(b) and 2(c). In this article, however, only the fundamental modes in rolled-up microcavities are considered because they can be treated using a two-dimensional model [15].

III. MODEL OF MODE SPLITTING

A clear physical model of mode splitting is crucial for angle-resolved nanoparticle sensing purposes. To address this problem, we developed a coupled-circular-waveguide model as shown in Fig. 3.

Due to the subwavelength-thin wall thickness commonly found in rolled-up microcavities, transverse magnetic (TM) polarized modes preferably exist as they possess better light confinement in the wall than transverse electric (TE) polarized modes [14,18]. Therefore, the scalar Helmholtz wave equation is applied for the z component $E_z(\rho,\theta)$ of the electric field:

$$-\frac{1}{n^2}\nabla^2 E_z(\rho,\theta) = k^2 E_z(\rho,\theta), \tag{1}$$

where n, k, and ∇^2 are the refractive index, the wave vector in vacuum, and the two-dimensional Laplace operator, respectively. Based on the adiabatic approximation [30], the

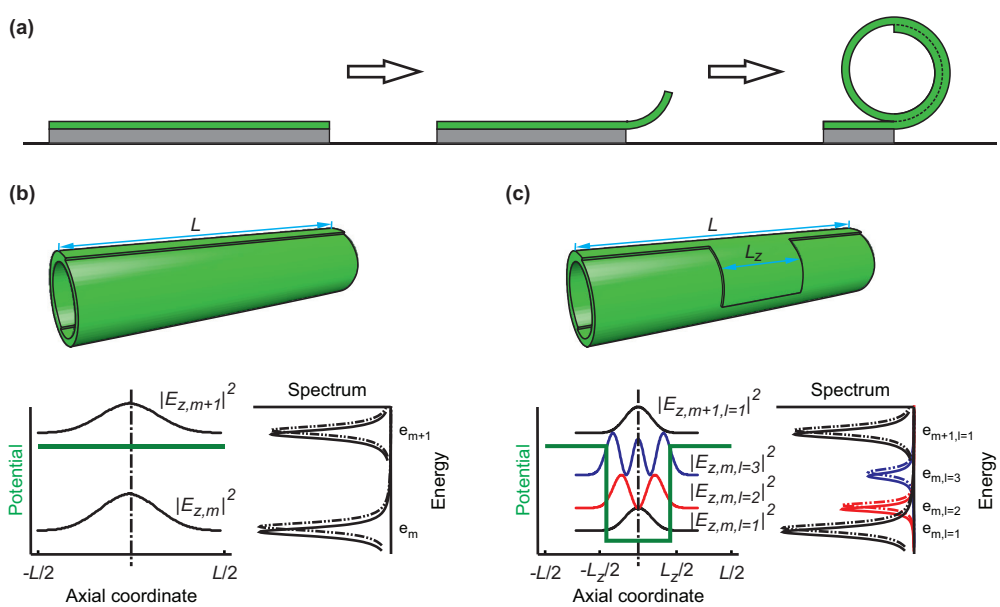

FIG. 2. (Color online) (a) Illustration of how nanomembranes are rolled up into tubular structures. A differentially strained nanomembrane (green, top layer) is deposited on a sacrificial layer (gray, bottom layer). The nanomembranes roll as the sacrificial layer is etched away creating an asymmetric tubular structure. The dashed line in (a) indicates the interface of the windings, where the surfaces of the membrane touch each other without gap. Illustrations of rolled-up microcavities without lobe structure (b) and with a rectangular-shaped lobe structure (c). The axial potential (thick green line) and resulting light axial field distribution (black lines for the fundamental modes and colored lines for the higher-order axial modes) are plotted in the lower left corner. In the lower right corner, corresponding spectra are shown. Intrinsic mode splitting due to the "steps" caused by the edges of the rolled membrane is shown with a dashed line.

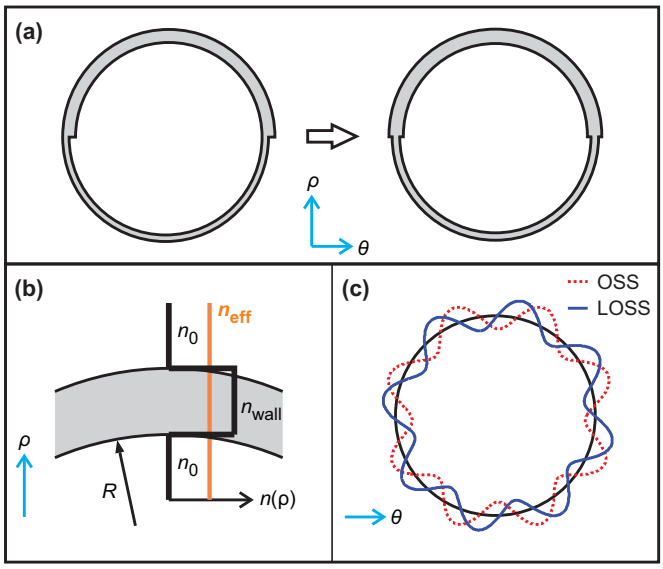

FIG. 3. (Color online) Coupled-circular-waveguide model of mode splitting in rolled-up optical microcavities. Diagram of (a) a rolled-up optical microcavity (left) that is equivalent to a coupled-circular waveguide (right) which is solvable using analytical and numerical methods, (b) profile of the refractive index $n(\rho)$ and the effective refractive index n_{eff}, and (c) electric field distribution along circumferential direction. The electric fields of the OSS mode are orthogonally distributed with respect to those of the LOSS mode.

electric field is treated as $E_z(\rho,\theta) = P(\rho)\Theta(\theta)$ and Eq. (1) becomes

$$\left[\rho^2\frac{d^2}{d\rho^2} + \rho\frac{d}{d\rho} + n^2(\rho)\frac{\omega^2}{c^2}\rho^2\right]P(\rho) = \beta^2 P(\rho), \tag{2}$$

$$\frac{d^2}{d\theta^2}\Theta(\theta) = -\beta^2\Theta(\theta), \tag{3}$$

where β is the propagation constant, which is solved numerically from Eq. (2) by introducing an effective refractive index n_{eff} such that $\beta = n_{\text{eff}}k$ [see details in Fig. 3(b)]. Then, the solution of Eq. (3) is expressed by $\Theta(\theta) = A\sin(\beta\theta + \varphi)$ with the amplitude A and the phase φ. To satisfy the continuity of the electric field $\Theta(\theta)$ at the two steps, we have

$$n_{\text{eff},1}L_1 + n_{\text{eff},2}L_2 = m\lambda, \tag{4}$$

$$\varphi_2 = \varphi_1 - \beta_2(L_1 + L_2), \tag{5}$$

where L, m, and λ are the length of the coupled-circular waveguide, the azimuthal mode number, and the wavelength in vacuum, respectively. The subscript indices 1 and 2 distinguish the variables in the thick- and thin-wall part. Equation (4) is the key equation to obtain the resonant modes in rolled-up microcavities [18]. Equation (5) describes the phase relation of the electric fields in the coupled-circular waveguide. The phase (e.g., φ_1) is determined by minimizing the Hamiltonian U of the system [30]:

$$U(\varphi_1) = \frac{\int |\nabla \times \Theta(\theta;\varphi_1)|^2 d\theta}{\int n^2|\Theta(\theta;\varphi_1)|^2 d\theta}. \tag{6}$$

In principle, there exists a certain phase which minimizes Eq. (6) that is the lowest energy mode of the system, called the lowest occupied standing-wave state (LOSS). Since the set of modes allowed by a cavity system are orthogonal to each other [31], the next highest mode is orthogonal to the LOSS and is called the orthogonal standing-wave state (OSS). The LOSS and OSS have different electric field distributions along the coupled-circular waveguide [see Fig. 3(c)], resulting in different resonant energies. Such a difference in energy is spectrally expressed as the mode splitting in rolled-up optical microcavities.

An asymmetric microcavity rolled from a 40-nm-thick nanomembrane, with an average refractive index of 1.9, 3.5 windings, and a diameter of 2 μm is used throughout this work. In this case, the nanomembrane is a square-shaped (22 μm × 22 μm) piece of dielectric material which after rolling results in a structure with a total wall thickness of 120 nm on half of the circumference and 160 nm on the other half. These parameters are typical for rolled-up microcavities [15,20]. Rolled-up microcavities can be fabricated so that portions of the structure are free-standing from the substrate, or lifted off of the substrate using a tapered fiber. Separation from the substrate is assumed in our calculations. Then, the effective refractive indices in the thick-wall part, $n_{\text{eff},1} = 1.60$, and in the thin-wall part, $n_{\text{eff},2} = 1.49$, were calculated according to Eq. (2). The Hamiltonian in Eq. (6) was cast as a function of the phase φ_1 and the result of this calculation is shown in Fig. 4. The phase φ_1 was determined, $\varphi_1 = 2.50$ rad, which corresponds to the LOSS mode with a minimum energy of $e_{\text{LOSS}} = 2.1718$ eV as well as the correlating total electric field [see Fig. 4(b)]. The OSS mode has the phase $\varphi_1 = 0.92$ rad with the maximum energy $e_{\text{OSS}} = 2.1746$ eV, and a corresponding total electric field as shown in Fig. 4(b). Altogether, an energy splitting of 2.8 meV at $m = 17$ is obtained.

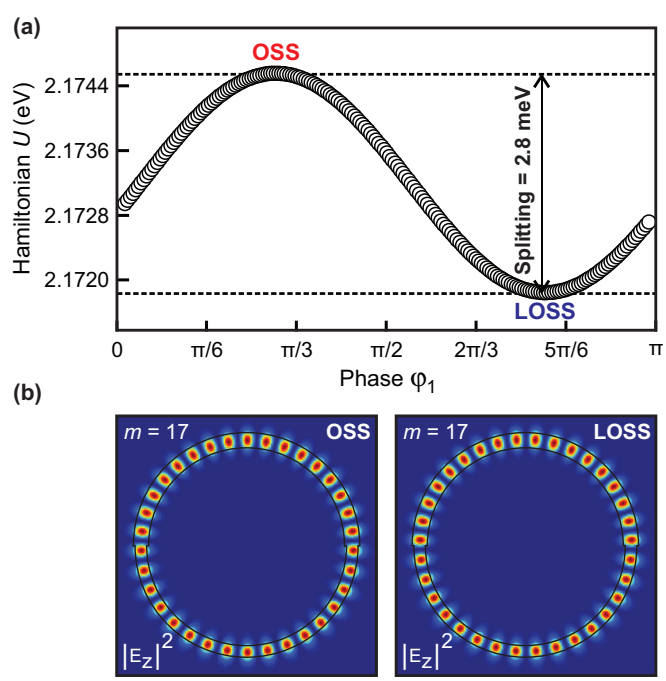

FIG. 4. (Color online) Calculated Hamiltonian U as a function of the phase φ_1 (a) and electric fields of the split modes (b). The electric field plots for the OSS and LOSS modes as determined by the calculation plotted in (a).

IV. EFFECT OF A SINGLE NANOPARTICLE ON MODE SPLITTING

A. Results of perturbation theory

In 2007, intrinsic mode splitting in an asymmetric sphere microcavity was systematically investigated by means of a near-field probe technique [13]. It was shown that the energies of the split modes periodically shift in opposite directions as the tip of a glass fiber is moved just over the cavity's surface along the equator. We expect that the electric fields of the modes are locked to subtle geometric irregularities in such a cavity. Due to this locking, the modes can be perturbed by the probe without causing a redistribution of the electric fields allowing them to be tuned. Unfortunately, because irregularities appear randomly, the modes are not locked to the geometry in a predictable way. This makes prediction of the shift without probing it impossible.

As mentioned previously, rolled-up microcavities have a well-defined asymmetry. In addition, the split modes in a rolled-up microcavity can be calculated based on the coupled-circular-waveguide model described in Sec. III. Perturbation theory [32] is therefore applied to predict the shifts of the split modes caused by the presence of a single nanoparticle on the resonator surface:

$$\Delta\omega = -\frac{\omega}{2}\frac{\langle E_z|\Delta n^2|E_z\rangle}{\langle E_z|n^2|E_z\rangle}, \tag{7}$$

where n, ω, and E_z are the refractive index, resonant angular frequency, and total electric field in the rolled-up microcavity without the nanoparticle, all of which are calculated by the coupled-circular-waveguide model. Δn is the variation of the refractive index induced by the nanoparticle. As long as the size and the position of the nanoparticle are known, the angular frequency shift $\Delta\omega$ of the split mode can be calculated. Combining the models based on variation and perturbation theories, the energy shifts of split modes in rolled-up microcavities are predictable.

Two major effects of the nanoparticle on the split modes are pointed out here, illustrated in Fig. 5. First, for a given azimuthal mode m, the two energies of the split mode synchronously shift as a function of the angular position of the nanoparticle. The two components shift periodically with a phase difference of π [see details in Fig. 5(a)]. Therefore, only one of the split modes (we take OSS mode) is needed for angle-resolved nanoparticle sensing purposes. Second, for neighboring azimuthal modes m and $m-1$, the energy shifts of the same split modes are out of synchronization [see details in Fig. 5(b)]. This effect will be used to uniquely detect the single nanoparticle's angular position.

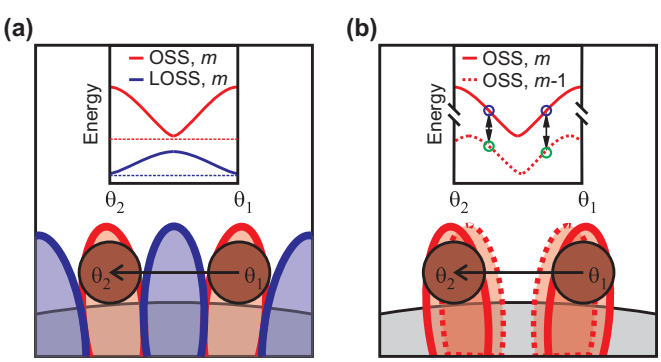

FIG. 5. (Color online) Schematics showing the resonant energy tuning caused by the nanoparticle (a) on the split modes and (b) on the same split mode at neighboring azimuthal modes. The blue (dark gray) and red (light gray) patterns indicate the electric fields of the LOSS mode and the OSS mode.

B. Verification by FDTD simulation

In addition to the analytical models used to calculate the split modes based on variational and perturbation theories, FDTD simulations [30] were also performed. These calculations allow us to ensure that perturbation methods are appropriate for our model, and to check that our analytical model agrees with a more complete depiction of the original rolled-up structure. In all FDTD simulations, a test nanoparticle having a diameter of 80 nm and a refractive index of 1.9 was used. Modes lying in the visible range ($m = 16$, 17, 18, and 19) were selected because they are the most useful in optical detection applications.

It was found that the modes split differently depending on the nanoparticle's angular position, which is defined as the number of degrees the nanoparticle is away from the outer step in the counterclockwise direction [see Fig. 6(a)]. Figure 6(b) shows the $m = 17$ mode in the absence of the nanoparticle and at two different angular positions. This position-dependent splitting is in contrast to a symmetric microcavity which, when a nanoparticle is attached, displays a mode splitting independent of the angular position of the nanoparticle [6,11].

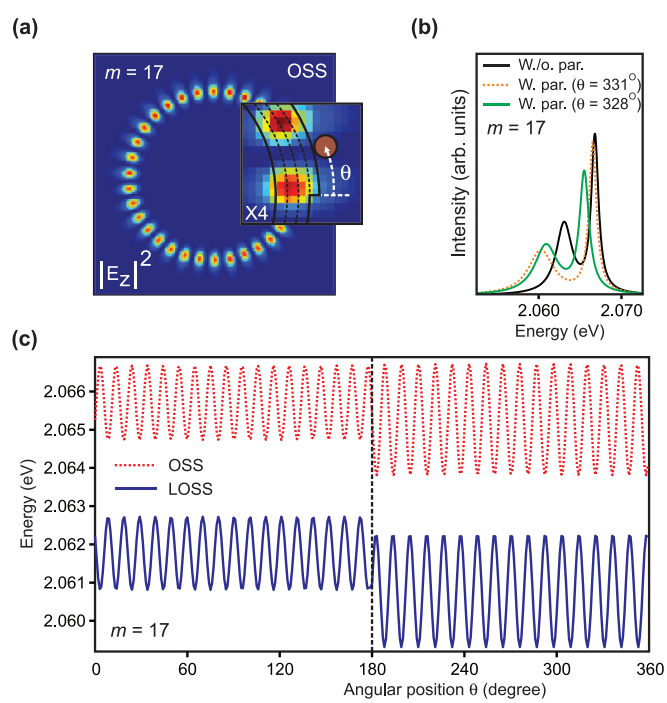

FIG. 6. (Color online) (a) Electric field profile of the OSS mode for $m = 17$. The location of a nanoparticle is defined by the azimuthal angle θ counterclockwise from the outside step. (b) Spectra for $m = 17$ in the absence of the nanoparticle, and with the nanoparticle at two different angular positions. (c) Resonant energies of the LOSS and the OSS modes as a function of the nanoparticle position.

The position independence in the symmetric microcavity arises due to the redistribution of the degenerate split modes, which are not locked to a particular feature of the structure. Hence, induced mode splitting in symmetric microcavities does not contain information about the nanoparticle's location. In a rolled-up microcavity, however, the single nanoparticle will modify the intrinsically split modes as a function of the angular position. Again, this is because the phase of the split modes is fixed to the steps in the structure, and the nanoparticle affects the LOSS and OSS modes to different degrees at a particular position.

Figure 6(c) shows how the splitting of the $m = 17$ mode varies as a function of angular position along the rolled-up microcavity. The evolution of each split mode exhibits periodic behavior. Several effects are observed which will be discussed one by one in the following. First, the magnitude of the modes' shift is greatest between 180° and 360°. This is the range of angles corresponding to the thin-wall part of the rolled-up microcavity where a stronger interaction between the nanoparticle and the resonant mode is present due to the more intense evanescent field on the microcavity surface. Second, the mode shifting oscillates as a function of angular position with an angular spatial frequency approximately equal to the mode index m, due to the perturbation of the nanoparticle in the periodic electric field. In the absence of a nanoparticle, the electric field distribution is predefined and locked by the steps in order to minimize the LOSS mode energy as described above. When a nanoparticle is introduced, it will disturb the electric field distribution. Due to the periodicity of the distribution, the nanoparticle will perturb the mode in a periodic way leading to an angular spatial frequency equal to the number of antinodes, which is close to the azimuthal mode index m. Third, the periodic tuning of the resonant mode energy shows an orthogonal evolution behavior between the LOSS and OSS modes. For example, the LOSS reaches a peak energy while the OSS reaches a minimum. Furthermore, the strongest interaction between the electric field and the nanoparticle is achieved when the nanoparticle is located at the antinode of the electric field. It was found that the results of FDTD simulations are consistent with our analytical models.

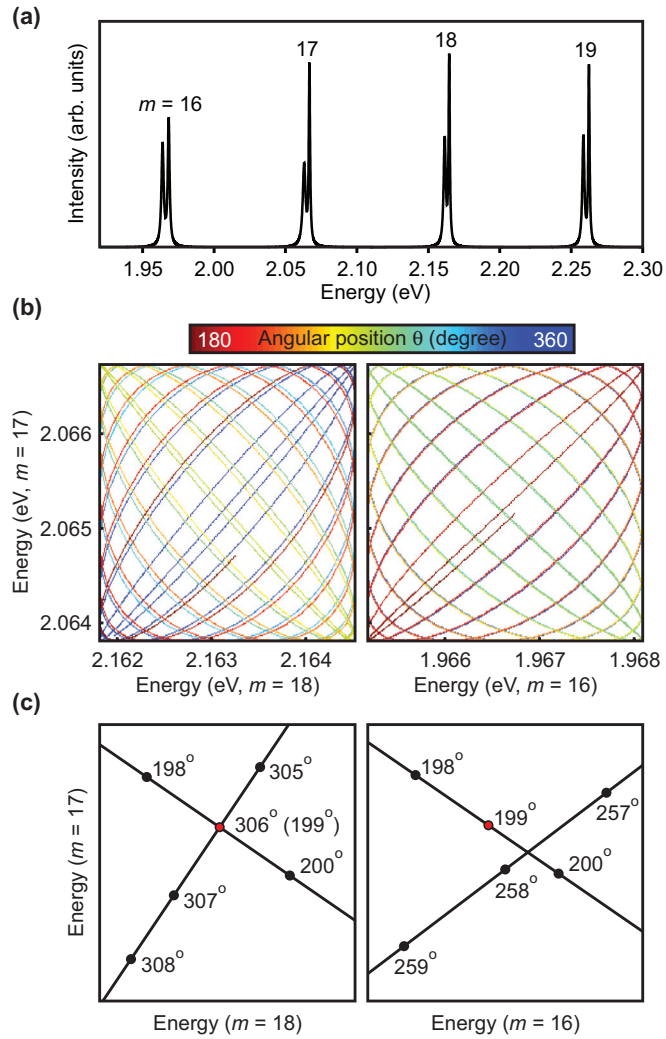

FIG. 7. (Color online) (a) Spectrum showing the mode splitting in four neighboring azimuthal modes. (b) Parametric plots of the resonant energies for the OSS mode at $m = 17$ combined with $m = 18$ (left) and $m = 16$ (right). (c) Local details of parametric plots in (b). The angular positions with an integer degree are depicted by the circles. The red circle highlights the cross point in the left. Knowledge of two resonant energies narrows the angular location down to one or two values. Using a third resonant energy the position is identified.

V. STRATEGY TO DETECT ANGULAR POSITION OF THE NANOPARTICLE

As shown in Fig. 6(c), and as discussed above, the LOSS and OSS components of a mode are directly related to one another, so use of only one component is sufficient. In addition, owing to the periodicity of the perturbation or tuning, it is clear that the angular position of a nanoparticle cannot be determined by monitoring only a single mode. Therefore a set of modes must be analyzed to determine a nanoparticle's position on the microcavity. Here the resonant energies of the OSS components of the $m = 16$, 17, and 18 modes were selected as shown in Fig. 7(a).

As we mentioned above, the mode energies oscillate as a function of angular position, with a periodicity related to the azimuthal mode number, and different azimuthal modes vary out of sync with each other (see Table I). Parametric plots of the resonant energies of $m = 17$ vs $m = 18$ as well as $m = 17$ vs $m = 16$ as a function of nanoparticle position illustrate this phenomenon, as shown in Fig. 7(b). This lack of synchronization may be exploited for detection purposes because it allows position information of the nanoparticle to be extracted from a set of resonant energies. Detection of angular position requires that the energies corresponding to the set of resonant energies should be unique to a particular position. For example, according to our parametric plots shown in Fig. 7(c) the resonant energies for the $m = 17$ and 18 modes yield possible angular position values of 199° or 306°, while the resonant energies for the $m = 17$ and 16 modes could only correspond to 199°. In this case, combining the set of modes, $m = 16$, 17, and 18, only one angular position is possible. Thus, by monitoring the resonant energies of three modes together, the spectroscopic detection of the angular position of a single nanoparticle on a rolled-up optical microcavity is demonstrated.

TABLE I. Fitting results for the simulated resonant energies, which are described by a cosine square function $e(\theta) = A\cos^2(\tilde{\omega}\theta + \theta_0) + e_0$. The subscript 1 (2) indicates the fitting parameter for the case that the nanoparticle is located at the thick-wall (thin-wall) part of the rolled-up microcavity.

	M	A_1 (meV)	$\tilde{\omega}_1$	$\theta_{0,1}$ (deg)	$e_{0,1}$ (eV)	A_2 (meV)	$\tilde{\omega}_2$	$\theta_{0,2}$ (deg)	$e_{0,2}$ (eV)
OSS	16	2.06	16.6	22	1.966	2.90	15.4	230	1.965
	17	1.95	17.6	28	2.065	2.91	16.4	237	2.064
	18	1.84	18.6	10	2.163	2.70	17.4	228	2.162
LOSS	16	2.18	16.6	308	1.961	3.09	15.4	141	1.960
	17	1.91	17.6	301	2.061	2.96	16.4	154	2.059
	18	1.82	18.6	285	2.159	2.78	17.4	144	2.158

VI. EXTENSION DISCUSSIONS

A. Diameter of the nanoparticle

As long as the mode splitting is periodically tuned by a single nanoparticle, the strategy to detect its angular position is available. In the following, the effect of nanoparticle size on the tuning behavior is studied in the selected angular position range and the results are shown in Fig. 8.

When the nanoparticle's size is smaller than 150 nm in diameter, the split mode is tuned in the same way but with different amplitude. Such nanoparticles are so "small" that they can be treated as a perturbation as we discussed above for the 80-nm particles. We simulated a further increase of the particle's size to around 170 nm, which is close to the half wavelength of the light used. An unstable tuning behavior (characterized by a tuning periodicity not equal to the azimuthal mode number) is observed due to strong Mie scattering from the nanoparticle [33], and we cannot detect the particle's angular position using our strategy. This size is the upper limit for perturbation calculations, which means that the nanoparticle cannot be treated as a perturbation any more. However, it is interesting that the periodic tuning behavior reappears when the particle's size increases further. This may be due to the redistribution and locking of split modes according to the steps as well as the nanoparticle. However, a detailed discussion of this effect is out of the scope of this article.

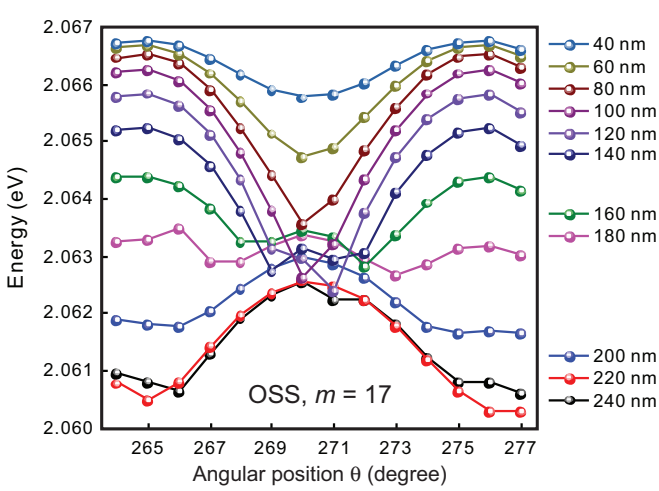

FIG. 8. (Color online) Resonant energy of the OSS mode at $m = 17$ as a function of the nanoparticle position with several sizes in diameter.

B. Axial confinement

In our analysis above, the microcavity, the electric field, and the nanoparticle are treated as a two-dimensional cross section. In three-dimensional space the nanoparticle would actually be a cylindrical rod. One could expect that the amplitude of the perturbation of a spherical nanoparticle is negligible in a cavity without axial confinement so that the proposed scheme of angular position detection is ineffective. However, this amplitude depends strongly on the overlap between the particle and the optical modes so it would be drastically enhanced when the mode is strongly confined in the axial direction.

Axial confinement and mode splitting have been experimentally demonstrated in a rolled-up microcavity with a rectangular-shaped lobe structure [15]. Figure 2(c) shows the axial electric field distribution within the lobe. The effective length of the confined electric field can be designed and treated as the length of the lobe L_z. When the axial size of a nanoparticle is comparable to L_z, the effect of the nanoparticle on the split modes reaches a maximum. Therefore, to achieve maximum sensitivity for angular position detection of a nanoparticle with a small axial size, a rolled-up microcavity with a similar scale of rectangular-shaped lobe structure is suggested.

C. Q-factor requirement

The detection of a single nanoparticle is available only if the splitting can be resolved in the spectrum. Higher Q-factor resonance peaks result in better-resolved peak splitting. Unfortunately, the Q factor is restrained due to the scattering by the steps and the nanoparticle. A detailed discussion about the Q-factor limitations in rolled-up optical microcavities has been reported in our previous work [23]. Here, however, we are interested in the lowest Q factor required to distinguish the split peaks which can be estimated by the Rayleigh criterion [34] by setting the full width at half maximum (FWHM) equal to the splitting for the two modes. The result is that the Q factor at the lower limit is about 1300 for the $m = 17$ mode which has a minimum splitting of 1.6 meV.

The presence of a nanoparticle on the microcavity will lead to a degradation of the Q factor due to Rayleigh scattering. Generally, the degree of the degradation is dependent on the size and the refractive index of the nanoparticle. However, in our case, the degradation of the Q factor also depends on the angular position. A nanoparticle located on the node or antinode will, respectively, lead to a minimum or maximum

degradation of the Q factor due to the scattering proportional to the intensity of the electric field.

VII. CONCLUSION

We have developed an analytical model of rolled-up optical microcavities, which provides useful insight into the physical cause of the mode splitting. Our model shows that the LOSS mode component is locked by the steps in the asymmetric structure, and that the OSS mode component is orthogonal to it. The influence a single nanoparticle has on the split modes was investigated. It was found that the nanoparticle's angular position periodically tunes the resonant mode energies with an angular spatial frequency proportional to the mode number m. By monitoring the resonant energies of three modes in concert with each other, determination of angular position of a single nanoparticle is possible. Based on this strategy, the functionality of optical microcavities as a detector is greatly enhanced.

ACKNOWLEDGMENTS

This work was supported by the Volkswagen Foundation (I/84072), the US Air Force Office of Scientific Research MURI program under Grant No. FA9550-09-1-0550, and the DFG priority Program No. FOR 1713. S.L.L. thanks the China Scholarship Council for financial support (CSC, File No. 2008617109). L.B.M. thanks the National Science Foundation of China (NSFC) for support through Grant No. 11104343. M.R.J. thanks the Alexander von Humboldt foundation for financial support.

APPENDIX: DEGENERACY LIFTING IN MICROCAVITIES

Consider a microcavity with a structural inhomogeneity Δn, under a mechanical rotation frequency Ω, as shown in Fig. 9(a). The degeneracy of two counterpropagating components (CW and CCW) is lifted via a backscattering mechanism caused by ring symmetry breaking (reciprocal process) [13] and, depending on experimental conditions, a reciprocity breaking process such as the Sagnac effect [35].

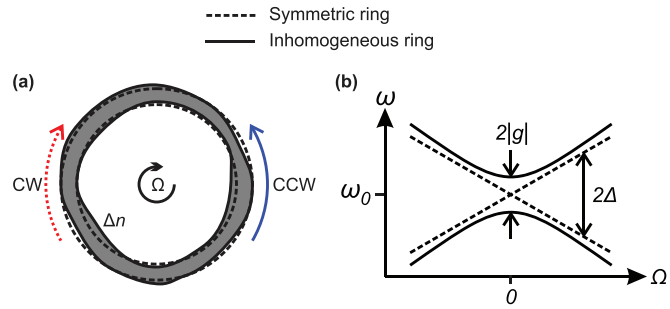

FIG. 9. (Color online) Coupled-modes theory for the pair of linearly coupled harmonic modes (CW and CCW components) with (a) a geometric schematic and (b) an eigenfrequency dispersion as a function of the mechanical rotation frequency Ω; see Ref. [12].

In the language of coupled-modes theory [12], the Heisenberg equation of motion of the complex amplitudes of CW and CCW components reads

$$i\frac{d}{dt}\begin{pmatrix} a_{\mathrm{CW}} \\ a_{\mathrm{CCW}} \end{pmatrix} = H\begin{pmatrix} a_{\mathrm{CW}} \\ a_{\mathrm{CCW}} \end{pmatrix} = \begin{pmatrix} \Delta & g \\ g^* & -\Delta \end{pmatrix}\begin{pmatrix} a_{\mathrm{CW}} \\ a_{\mathrm{CCW}} \end{pmatrix}, \tag{A1}$$

where g and Δ are the coupling and detuning coefficients caused by the backscattering in the reciprocal and nonreciprocal processes, respectively. It should be noted that the matrix H is Hermitian and the coupling is conservative here [12]. Diagonalization of H yields two normal components with eigenfrequencies $\omega = \omega_0 \pm \sqrt{|g|^2 + \Delta^2}$, where ω_0 is the degenerate eigenfrequency in symmetric ring structure without any mechanical rotation. The eigenfrequency dispersion is shown in Fig. 9(b) as function of the mechanical frequency Ω.

In the absence of mechanical rotation, reciprocity is maintained even though the CW and CCW components are no longer degenerate. We approached this problem using frequency-domain calculations and found that a split mode results from components that are standing waves locked into place by the structure's geometry. Because the two locked components have nodes located in different environments within the geometry, their energies are different.

[1] D. K. Armani, T. J. Kippenberg, S. M. Spillane, and K. J. Vahala, Nature (London) **421**, 925 (2003).
[2] F. Vollmer and S. Arnold, Nat. Methods **5**, 591 (2008).
[3] F. Vollmer, S. Arnold, and D. Keng, Proc. Natl. Acad. Sci. USA **105**, 20701 (2008).
[4] T. Lu, H. Lee, T. Chen, S. Herchak, J.-H. Kim, S. E. Fraser, R. C. Flagan, and K. J. Vahala, Proc. Natl. Acad. Sci. USA **108**, 5976 (2011).
[5] A. M. Armani, R. P. Kulkarni, S. E. Fraser, R. C. Flagan, and K. J. Vahala, Science **317**, 783 (2007).
[6] J. Zhu, S. K. Ozdemir, Y.-F. Xiao, L. Li, L. He, D.-R. Chen, and L. Yang, Nat. Photonics **4**, 46 (2010).
[7] J. Zhu, S. K. Ozdemir, L. He, D.-R. Chen, and L. Yang, Opt. Express **19**, 16195 (2011).
[8] L. He, S. K. Ozdemir, J. Zhu, W. Kim, and L. Yang, Nat. Nanotechnol. **6**, 428 (2011).
[9] K. J. Vahala, Nature (London) **424**, 839 (2003).
[10] M. Pöllinger, D. O'Shea, F. Warken, and A. Rauschenbeutel, Phys. Rev. Lett. **103**, 053901 (2009).
[11] T. J. Kippenberg, Nat. Photonics **4**, 9 (2010).
[12] R. J. C. Spreeuw and J. P. Woerdman, Physica B **175**, 96 (1991).
[13] A. Mazzei, S. Götzinger, L. De S. Menezes, G. Zumofen, O. Benson, and V. Sandoghdar, Phys. Rev. Lett. **99**, 173603 (2007).
[14] M. Hosoda and T. Shigaki, Appl. Phys. Lett. **90**, 181107 (2007).
[15] Ch. Strelow, C. M. Schultz, H. Rehberg, M. Sauer, H. Welsch, A. Stemmann, C. Heyn, D. Heitmann, and T. Kipp, Phys. Rev. B **85**, 155329 (2012).

[16] V. Y. Prinz, V. A. Seleznev, A. K. Gutakovsky, A. V. Chehovskiy, V. V. Preobrazhenskii, M. A. Putyato, and T. A. Gavrilova, Physica E **6**, 828 (2000).
[17] O. G. Schmidt and K. Eberl, Nature (London) **410**, 168 (2001).
[18] T. Kipp, H. Welsch, Ch. Strelow, C. Heyn, and D. Heitmann, Phys. Rev. Lett. **96**, 077403 (2006).
[19] R. Songmuang, A. Rastelli, S. Mendach, and O. G. Schmidt, Appl. Phys. Lett. **90**, 091905 (2007).
[20] G. S. Huang, S. Kiravittaya, V. A. B. Quinones, F. Ding, M. Benyoucef, A. Rastelli, Y. F. Mei, and O. G. Schmidt, Appl. Phys. Lett. **94**, 141901 (2009).
[21] S. Vicknesh, F. Li, and Z. Mi, Appl. Phys. Lett. **94**, 081101 (2009).
[22] J. Wang, T. Zhan, G. S. Huang, X. Cui, X. Hu, and Y. F. Mei, Opt. Express **20**, 18555 (2012).
[23] S. Böttner, S. Li, J. Trommer, S. Kiravittaya, and O. G. Schmidt, Opt. Lett. **37**, 5136 (2012).
[24] S. M. Harazim, V. A. B. Quinones, S. Kiravittaya, S. Sanchez, and O. G. Schmidt, Lab Chip **12**, 2649 (2012).
[25] L. Ma, S. Li, V. A. B. Quinones, L. Yang, W. Xi, M. R. Jorgensen, S. Baunack, Y. F. Mei, S. Kiravittaya, and O. G. Schmidt, Adv. Mater. **25**, 2357 (2013).
[26] P. Cendula, S. Kiravittaya, I. Mönch, J. Schumann, and O. G. Schmidt, Nano Lett. **11**, 236 (2010).
[27] P. Cendula, S. Kiravittaya, Y. F. Mei, C. Deneke, and O. G. Schmidt, Phys. Rev. B **79**, 085429 (2009).
[28] Z. Tian, V. Veerasubramanian, P. Bianucci, Z. Mi, A. G. Kirk, and D. V. Plant, Opt. Lett. **36**, 3506 (2011).
[29] Z. Tian, V. Veerasubramanian, P. Bianucci, S. Mukherjee, Z. Mi, A. G. Kirk, and D. V. Plant, Opt. Express **19**, 12164 (2011).
[30] J. D. Joannopoulos, S. G. Johnson, J. N. Winn, and R. D. Meade, *Photonic Crystals: Molding the Flow of Light* (Princeton University Press, Princeton, NJ, 2008).
[31] A. Hardy, P. A. Belanger, and A. E. Siegman, Appl. Opt. **21**, 1122 (1982).
[32] S. G. Johnson, M. Ibanescu, M. A. Skorobogatiy, O. Weisberg, J. D. Joannopoulos, and Y. Fink, Phys. Rev. E **65**, 066611 (2002).
[33] C. F. Bohren and D. R. Huffman, *Absorption and Scattering of Light by Small Particles* (Wiley-VCH Verlag GmbH, New York, 2007).
[34] F. Tamburini, G. Anzolin, G. Umbriaco, A. Bianchini, and C. Barbieri, Phys. Rev. Lett. **97**, 163903 (2006).
[35] R. J. C. Spreeuw, N. J. van Druten, M. W. Beijersbergen, E. R. Eliel, and J. P. Woerdman, Phys. Rev. Lett. **65**, 2642 (1990).